Estimating the 3D structure of the Enceladus ice shell from flexural and Crary waves

A.G. Marusiak [1]*,S. Tharimena [1], M.P. Panning [1], S.D. Vance, [1], C. Boehm [2], S. Stähler[2], M. Van Driel [3]

[1]Jet Propulsion Laboratory, California Institute of Technology
[2]Institute for Geophysics, ETH Zürich
[3]Carl Zeiss SMT GmbH

Key Points:

- 3D models of the Enceladus ice shell are used to test best methods for constraining the ice shell structure.
- Flexural waves dominate if ice shells are thinner than 20 km, otherwise Rayleigh waves will dominate.
- The frequency content of the Crary wave depends on the average ice shell thickness.

*Now at USGS Earthquake Science Center

Corresponding author: A.G. Marusiak, angela.marusiak@gmail.com

Abstract

A seismic investigation on Saturn's moon Enceladus could determine the thickness of the ice shell, along with variations from the mean thickness, by recovering phase and group velocities, and through the frequency content of surface waves. Here, we model the Enceladus ice shell with uniform thicknesses of 5 km, 20 km, and 40 km, as well as with ice topography ranging from 5-40 km. We investigate several approaches for recovering the mean ice shell thickness. We show that surface wave dispersions could be used to determine the mean ice shell thickness. Flexural waves in the ice only occur if the shell is thinner than a critical value < 20 km. Rayleigh waves dominate only in thicker ice shells. The frequency content of Crary waves depends on the ice shell thickness.

Plain Language Summary

Saturn's moon, Enceladus, has a surface ice shell that likely varies in thickness from about 5km to 40 km. Seismology could be used to determine where the ice shell is relatively thin or thick, and constrain the average ice shell thickness. We created models of the Enceladus ice shell with constant thicknesses of 5, 20, and 40 km, and a fourth model which had variable ice shell thickness. The variable thickness represents the predicted ice shell topography. These models help us develop the best approaches for recovering Enceladus' ice shell structure. We find surface wave dispersion, flexural waves, and Crary wave properties vary based on ice shell thickness, and thus can be used to reveal the ice shell structure.

1 Introduction

Saturn's moon Enceladus has the best characterized ocean of the many discovered ocean worlds (Hendrix et al., 2018; National Academies of Sciences Engineering and Medicine, 2022), and is a high priority target for future exploration. Planned and studied missions to land on Titan (Barnes et al., 2021), Enceladus (Mackenzie et al., 2021), and Europa (Hand et al., 2017) include seismic payloads, similar to the seismic experiment on the InSight mission to Mars (Lognonné et al., 2019). Tidally flexed ocean worlds are anticipated to provide abundant seismic data that will be important for revealing internal mechanical and thermal structure (Marusiak et al., 2021; S. D. Vance, DellaGiustina, et al., 2021; S. D. Vance, Behounkova, et al., 2021; Kovach & Chyba, 2001; Pappalardo et al., 2013). These constraints are needed to determine whether subsurface oceans are or were habitable (S. D. Vance et al., 2018). The main source of seismicity is likely tidal flexing (Hurford et al., 2020), including hydrothermal or volcanic activity at the base of the ocean (Waite et al., 2017; Choblet et al., 2017), and fluid motions as material is exchanged between the surface, ice shell, and ocean.

Here, we investigate different approaches and methods for constraining the ice shell thickness of Enceladus using seismology. Previous studies (e.g. (Maguire et al., 2021; Lee et al., 2003; Stähler et al., 2017)) have focused on using simple one-dimensional modeling. However, the Cassini mission provided evidence for spatial variability in the thickness of the Enceladus ice shell, particularly with latitude (Čadek et al., 2016; Beuthe, 2018; Iess et al., 2014; McKinnon, 2015) (Figure 1a).

Due to its small radius of 252 km, surface waves on Enceladus can easily orbit the moon multiple times within $\leq$800 s. Rayleigh waves with wavelengths less than the ice shell thickness show little dispersion and will travel with speeds equal to 0.92 the shear wave velocity (Vs). Flexural surface waves—those with wavelengths greater than the thickness of the ice—perturbed by the base of the ice shell will travel as full layer waves. These waves have intrinsic dispersion that depends on the velocity gradient in the ice. It is expected that thin ice shells will cause flexural waves to dominate the seismic records. In addition to flexural waves, we anticipate to observe Crary waves (Crary, 1954). Crary

waves (Cr) are monochromatic trapped waves that have a phase velocity equivalent to compressive velocities (Vp) and have characteristic harmonic frequency spectra (Equation 1) dependent on the ice shell thickness. The frequency content of the Crary wave spectrum along with the dispersion of surface waves and the transition of Rayleigh to flexural waves can be used to determine the ice shell thickness (Stähler et al., 2017).

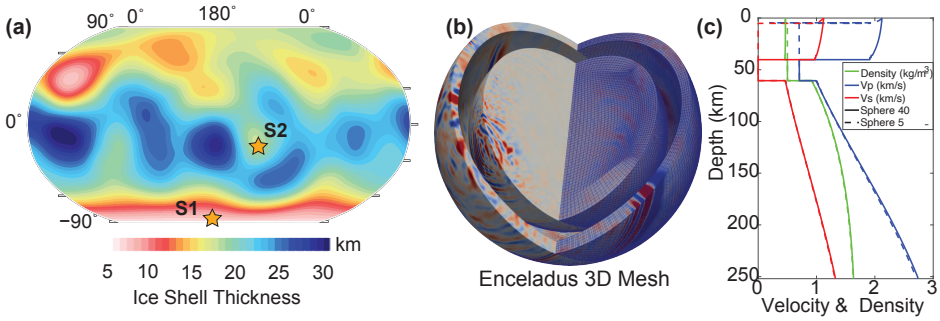

Figure 1. Interior structure of Enceladus based on (Čadek et al., 2016). (see Methods) a) The ice shell thickness is allowed to vary laterally, with thinnest ice at poles and thickest ice near the equator. Two possible source locations (S1 and S2) are shown. b) The associated 3D mesh used to model the full seismic waveforms.Colors represent motion from a simulated encelaquake. c) Representative internal structures and wave velocities in 1D cross-section.

2 Methods

We build one-dimensional models with uniformly thick ice shells of 5, 20, and 40 km (Čadek et al., 2019; Běhounková et al., 2017; Čadek et al., 2016; Olgin et al., 2011; Lucchetti et al., 2017)(Figure 1a), and one model with topography built into the ice shell such that the thickness varies laterally ranging from 5 to 40 km allowing for more realistic 3D simulations (Figure 1 b). We use PlanetProfile (S. D. Vance et al., 2022, 2018) to generate geophysically-consistent interior structure models of Enceladus including the physical and bulk properties (Figure 1c). PlanetProfile calculates geophysically consistent radial models, and calculates the seismic profile based on the SeaFreeze library (Journaux et al., 2020). PlanetProfile has been previously used to model seismic responses for Europa (Panning et al., 2018; Marusiak, Panning, et al., 2022), Titan (Marusiak, Vance, et al., 2022), and icy ocean worlds in general (Stähler et al., 2017). We maintain the same silicate, ocean and ice compositions for each of the models to maintain consistency, though the composition beneath the ice shell is somewhat arbitrary as we focus on the seismic wave propagation in the ice shell. We assume the ice shell is composed of pure water ice Ih for simplicity. Once we have the basic one-dimensional models, we extrapolate the results to create a three-dimensional model with laterally varying ice shell thickness. The ice surface topography is derived from measurements using Cassini's laser altimeter (Tajeddine et al., 2017). The ice-ocean boundary topography is derived from gravity data (Čadek et al., 2016, 2019) . The interior structure models from PlanetProfile are used as inputs to create synthetic waveforms.

We create the synthetic waveforms using the Salvus software from Mondaic (Afanasiev et al., 2019). Our meshes (Figure 1b) have a global resolution of 5 s and 3 s allowing us to incorporate the variations in ice shell thickness. We use Salvus to create models with 5 km, 20 km, 40 km thick ice, as well as a global model with varying ice shell thickness. Our source is a Mw 3.4, double-couple source (S1) as well as a real moment tensor from Lake Tanganyika (GMCTID: C201702240032A) (S2) scaled to be a Mw 3.4. Both were

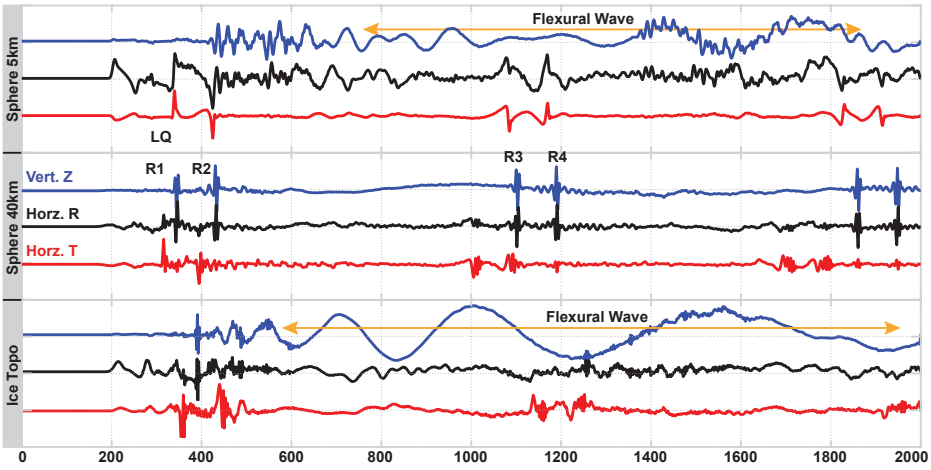

Figure 2. Ground motions in the vertical (blue), horizontal radial (black) and horizontal transverse (red) directions for an event with a depth of 3 km, Mw 3.4, and the moment tensor from the Lake Tanganyika event. The receiver is set at an epicentral distance of 160°. The ground displacement normalized to the maximum value is shown for a 5 km (top), 40 km (middle), and variable ice thickness (bottom) models. Key surface waves such R1, R2, R3, and R4 are labeled. The flexural wave (orange arrows) are shown for the thin and variable thickness models.

set at a depth of 3 km, within the ice shell. We set receivers to be globally located and spaced 1° apart.

We set the seismograms to be 2000 s in length, which allows us to capture flexural waves and Rayleigh waves that travel along major arcs (R1) and minor arcs (R2) multiple times around Enceladus (Rn) (Figure 2).

3 Results

The ground motion and seismic responses for different ice shell models will reveal which approaches and seismic waves best constrain ice shell thickness.

3.1 Time-Series Analysis

Figure 2 shows example seismic records of ground displacement for the different models. The source occurs at (-17, 218) and the receiver is about 160°away at (20, 60). The Rayleigh waves are easily identifiable on the thicker and variable thickness models. However, the flexural wave is best seen with thin or variable thickness models. Because the thickness of the ice is greater than the wavelength of the surface waves, the flexural wave is not visible for thick ice, and its absence allows for the R3 and R4 Rayleigh waves to be revealed. Including ice shell topography allows both R1, R2, and flexural waves to be seen, but the seismograms do have more dispersive energy, producing weaker ground motions compared to uniform ice shells.

The differences in seismic phases are further revealed by examining the moveout of key seismic phases in distance and time (Figure 3). Including under-ice topography tends to reduce amplitudes compared to models with uniform ice shell thickness. The thinner ice shell has stronger motion in the horizontal component for events within ≈ 50° of the receiver. This short separation can obscure some of the body phases, includ-

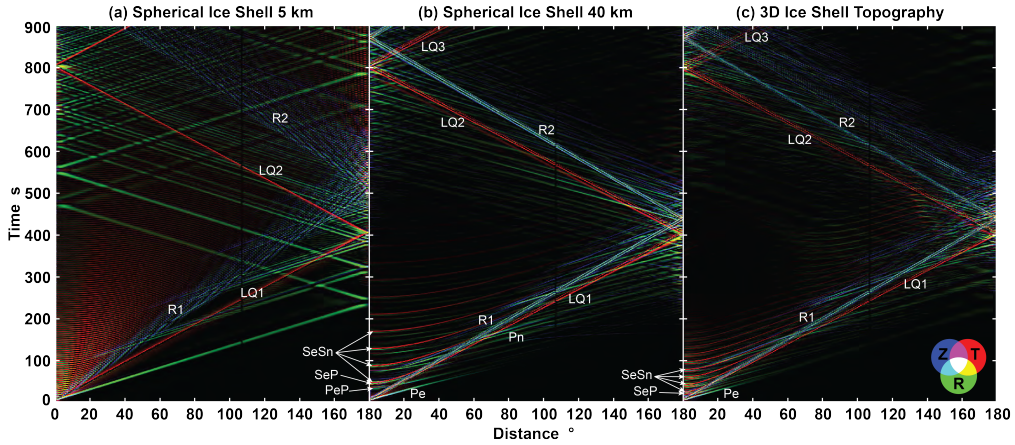

Figure 3. Ground motions in the vertical (blue), horizontal radial (green) and horizontal transverse (red) directions for an event with a depth of 3 km, Mw 3.4, and the moment tensor from the Lake Tanganyika event. Time (s) is plotted on the y-axis, epicentral distance (°) on the x-axis, and the intensity of the color indicates the amount of ground displacement recorded on the three components. White indicates strong motion on all three components. Panels show resulting ground displacements for ice shell thicknesses of a) 5 km, b) 40 km, and c) for variable ice shell thickness.

ing reflections off the ice shell (e.g. SeS, SeP, PeP, see Stähler et al. (2017)) that are more easily observable on thicker ice shells, or in models with surface topography. The ice shell reflections could be used to determine the thickness of the ice shell at the points of reflection, providing additional data to constrain the average ice shell thickness. If the locations of multiple seismic events are well constrained, the recovered ice shell thicknesses from the ice reflections could be used to map variations in the ice shell thickness.

3.2 Surface Wave Dispersion

The spectra of seismograms also highlight differences among the models (Figure 4). The flexural wave is more clearly visible in models with thin ice shells and has the strongest signal. In thicker ice shells, the flexural wave is not clearly seen, however the Rayleigh waves are identifiable. Rayleigh waves dominate at periods between 5-20 s. In the model with ice topography, the transition is seen between Rayleigh and flexural waves at periods of $\geq$ 20 s.

We show that our picked group velocities match those predicted by the Mineos software package (Masters et al., 2011) for periods greater than $\approx$ 20 s for the 5 km uniform ice shell (Figure 5). In our model with ice topography, the group velocities are close to the dispersion curve for a 20 km ice shell. This result is not surprising, as the mean ice shell thickness was 17-20 km depending on the receiver location. For the thinner 5 km ice shell, the group velocity is about 1.5 km/s for periods less than 20 s. For the model with under-ice topography, the group velocity is about 1.5 km/s for periods less than $\approx$ 75 s. The results indicate that group velocities can be used to recover mean ice thickness for given travel paths.

Crary waves can also constrain the ice shell thickness. We use the spectra for a window of time surrounding the Crary wave arrival to compare the differences among the models. We calculate the frequency of the Crary wave by assuming a Vp value of 3.9 km/s, and a Vs value of 1.97 km/s (Equation 1). The predicted Crary wave frequencies are shown

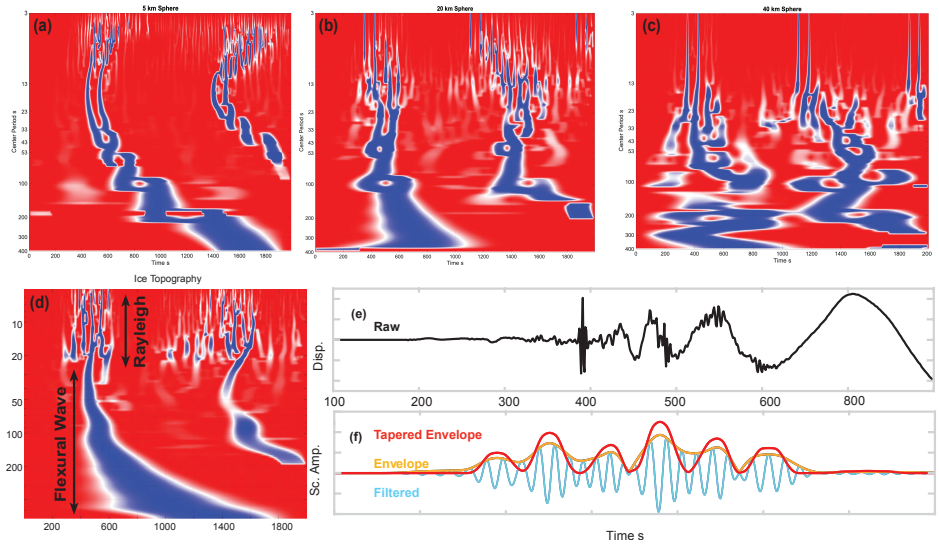

Figure 4. An event occurring at a distance of 160°. Stacked spectra of the surface waves are shown for uniform ice shell thicknesses of a) 5 km, b) 20 km, c) 40 km, and d) the model with ice topography. The spectra are created by taking raw seismograms (e, black) using a narrow band Gaussian bandpass filter centered at 17.8 s (f, cyan), and then computing envelopes of energy packets to estimate the dispersion of the surface waves (f, orange). The tapered envelope (f, red) helps to separate phases and is used to create stacks (a-d) based on time (x-axis) and period (y-axis).

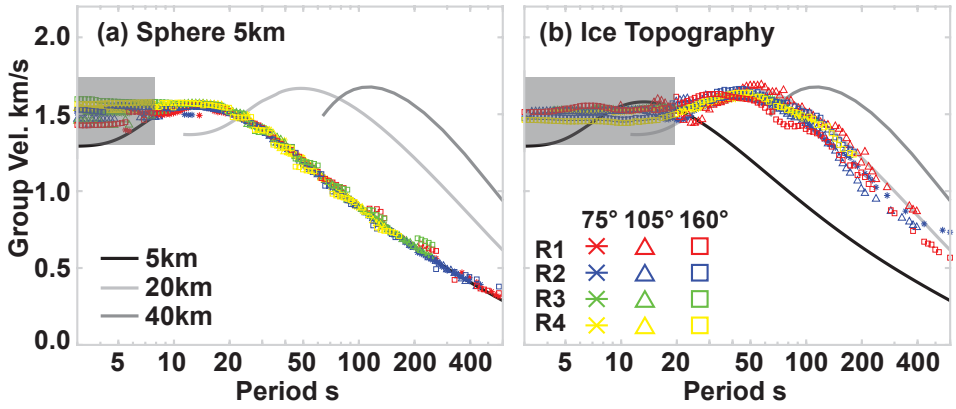

Figure 5. Group velocities for 3 receivers at 75°(cross), 105°(triangle), and 160°(square) from the source, computed using the dispersion curves in Figure 4. Solid curves represent the group velocity curves for 5 km (black), 20 km (light gray), and 40 km (dark gray) ice shell models. a) The dispersion curves for a 5 km thick ice shell. b) Model with ice topography. The mean ice shell thickness is 20 km, 19 km, 18 km, and 17 km thick for receivers R1 (red), R2 (blue), and R3 (green), and R4 (yellow) respectively. The shaded gray box indicates where the recovered group velocities vary from the theoretical group velocities.

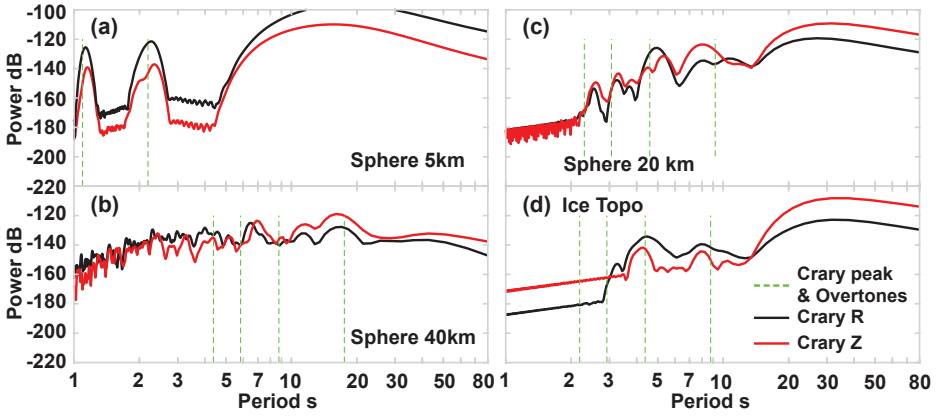

Figure 6. Periodograms of the vertical (red) and radial (blue) components for models with ice shell thickness of a) 5km, b) 40 km, c) 20 km and d) with ice topography. A time window was applied surrounding the predicted Crary wave arrival. Dashed green vertical lines represent the calculated frequencies for Crary waves using Equation 1.

as dashed green lines in Figure 6. Thin ice shells (< 20 km) match the predicted resonant frequencies, but the thicker ice don't necessarily show strong peaks everywhere they were predicted. Furthermore, the model with variable ice shell thickness produces periodograms similar to, but not matching exactly, the model with a uniform 20 km ice shell.

$$f_{\mathrm{Cr}} = \frac{(n+1)v_S}{2d\sqrt{1-\left(\frac{v_S}{v_P}\right)^2}}, \tag{1}$$

4 Discussion

We investigate different approaches for recovering the ice shell thickness from several models. By creating one model with ice topography, thus variable ice shell thickness, we can better compare which methods can be used to recover mean ice shell thickness. We show that the presence, or lack thereof, of flexural waves and Rayleigh waves can indicate relative thickness of the ice shell. Depending on the source-to-receiver distance and the thickness of the ice shell, we anticipate different waves should dominate the seismic records. Thinner ice shells will show strong flexural waves, but may obscure reflected body waves. Thicker ice shells are more likely to produce strong Rayleigh waves and allow for the observation of more body waves (depending on distance from the event). Body waves, including reflections off the ice-ocean interface, could be used to infer the thickness of the ice shell at the bounce point. The use of surface waves dispersions will likely yield the thickness of the ice shell. This finding is consistent with previous studies on Europa (Maguire et al., 2021) that also explore the role of surface wave dispersion for recovering ice shell thickness. We show that the frequency content and group velocity of the surface waves will reveal the mean ice shell thickness along the travel path from the source to receiver. For a model with variable ice shell thickness, comparisons of dispersion from different events could indicate regions, or least the relative directions, where the ice varies from the mean thickness.

5 Conclusion

We show that time-series and spectral analysis of surface waves can best recover mean ice shell thickness for the icy-ocean world, Enceladus. Our model with variable ice shell thickness included both rayleigh and flexural wave arrivals. The frequency content of these waves can be used to constrain mean ice shell thickness. The dispersion curves for these waves can further indicate the mean ice shell thickness along the travel path of the seismic waves.

6 Open Research

Raw seismograms and mineos results are available on Zenodo (doi: 10.5281/zenodo.7023774, https://zenodo.org/record/7023774.Yw0cZh3MJYg) PlanetProfile code is downloadable through Github (S. Vance, 2017). Salvus scripts are available upon request and require an active license to run.

Acknowledgments

A part of the research was carried out at the Jet Propulsion Laboratory, California Institute of Technology, under a contract with the National Aeronautics and Space Administration (80NM0018D0004). Work by JPL authors was supported by a grant from NASA's Habitable Worlds program (16-HW16_2-0065). Copyright 2022.

References

Afanasiev, M., Boehm, C., van Driel, M., Krischer, L., Rietmann, M., May, D. A., ... Fichtner, A. (2019, 3). Modular and flexible spectral-element waveform modelling in two and three dimensions. *Geophysical Journal International*, *216*(3), 1675–1692. Retrieved from https://doi.org/10.1093/gji/ggy469 doi: 10.1093/gji/ggy469

Barnes, J. W., Turtle, E. P., Trainer, M. G., Lorenz, R. D., MacKenzie, S. M., Brinckerhoff, W. B., ... Stähler, S. C. (2021, 8). Science Goals and Objectives for the Dragonfly Titan Rotorcraft Relocatable Lander. *The Planetary Science Journal*, *2*(4), 130. Retrieved from http://dx.doi.org/10.3847/PSJ/abfdcfhttps://iopscience.iop.org/article/10.3847/PSJ/abfdcf doi: 10.3847/PSJ/abfdcf

Běhounková, M., Souček, O., Hron, J., & Čadek, O. (2017, 8). Plume Activity and Tidal Deformation on Enceladus Influenced by Faults and Variable Ice Shell Thickness. *Astrobiology*, *17*(9), 941–954. Retrieved from https://doi.org/10.1089/ast.2016.1629 doi: 10.1089/ast.2016.1629

Beuthe, M. (2018, 3). Enceladus's crust as a non-uniform thin shell: I tidal deformations. *Icarus*, *302*, 145–174. Retrieved from https://www.sciencedirect.com/science/article/pii/S0019103517304402?_rdoc=1&_fmt=high&_origin=gateway&_docanchor=&md5=b8429449ccfc9c30159a5f9aeaa92ffb&dgcid=raven_sd_via_email doi: 10.1016/J.ICARUS.2017.11.009

Čadek, O., Souček, O., Běhounková, M., Choblet, G., Tobie, G., & Hron, J. (2019, 2). Long-term stability of Enceladus' uneven ice shell. *Icarus*, *319*, 476–484. Retrieved from http://www.sciencedirect.com/science/article/pii/S0019103518303762https://linkinghub.elsevier.com/retrieve/pii/S0019103518303762 doi: 10.1016/j.icarus.2018.10.003

Čadek, O., Tobie, G., Van Hoolst, T., Massé, M., Choblet, G., Lefèvre, A., ... Bourgeois, O. (2016). Enceladus's internal ocean and ice shell constrained from Cassini gravity, shape, and libration data. *Geophysical Research Letters*, *43*(11), 5653–5660.

Choblet, G., Tobie, G., Sotin, C., Běhounková, M., Čadek, O., Postberg, F., & Souček, O. (2017). Powering prolonged hydrothermal activity inside Enceladus. *Nature Astronomy*, *1*(12), 841–847. Retrieved from https://doi.org/10.1038/s41550-017-0289-8 doi: 10.1038/s41550-017-0289-8

Crary, A. P. (1954). Seismic studies on Fletcher's Ice Island, T-3. *Transactions, American Geophysical Union*, *35*(2), 293. Retrieved from http://dx.doi.org/10.1016/j.biotechadv.2010.07.003%0Ahttp://dx.doi.org/10.1016/j.scitotenv.2016.06.080%0Ahttp://dx.doi.org/10.1016/j.bbapap.2013.06.007%0Ahttps://www.frontiersin.org/article/10.3389/fmicb.2018.02309/full%0Ahttp://dx.doi.org/10.1007/s13762- doi: 10.1029/TR035i002p00293

Hand, K. P., Murray, A. E., Garvin, J. B., Brinckerhoff, W. B., Christner, B. C., Edgett, K. S., ... Team, P. E. (2017). *Report of the Europa Science Definition Team* (Tech. Rep.). Retrieved from https://europa.nasa.gov/resources/58/europa-lander-study-2016-report/

Hendrix, A. R., Hurford, T. A., Barge, L. M., Bland, M. T., Bowman, J. S., Brinckerhoff, W., ... Vance, S. D. (2018, 10). The NASA Roadmap to Ocean Worlds. *Astrobiology*, *19*(1), 1–27. Retrieved from https://doi.org/10.1089/ast.2018.1955 doi: 10.1089/ast.2018.1955

Hurford, T. A., Henning, W., Maguire, R., Lekic, V., Schmerr, N. C., Panning, M. P., ... Rhoden, A. (2020, 3). Seismicity on tidally active solid-surface worlds. *Icarus*, *338*, 113466. Retrieved from http://www.sciencedirect.com/science/article/pii/S0019103518307243https://linkinghub.elsevier.com/retrieve/pii/S0019103518307243 doi: 10.1016/j.icarus.2019.113466

Iess, L., Stevenson, D. J., Parisi, M., Hemingway, D., Jacobson, R. A., Lunine, J. I., ... Tortora, P. (2014, 4). The Gravity Field and Interior Structure of Enceladus. *Science*, *344*(6179), 78–80. Retrieved from https://www.sciencemag.org/lookup/doi/10.1126/science.1250551 doi: 10.1126/science.1250551

Journaux, B., Brown, J. M., Pakhomova, A., Collings, I. E., Petitgirard, S., Espinoza, P., ... Hanfland, M. (2020, 1). Holistic Approach for Studying Planetary Hydrospheres: Gibbs Representation of Ices Thermodynamics, Elasticity, and the Water Phase Diagram to 2,300 MPa. *Journal of Geophysical Research: Planets*, *125*(1), e2019JE006176. Retrieved from https://doi.org/10.1029/2019JE006176https://onlinelibrary.wiley.com/doi/10.1029/2019JE006176 doi: 10.1029/2019JE006176

Kovach, R. L., & Chyba, C. F. (2001, 4). Seismic Detectability of a Subsurface Ocean on Europa. *Icarus*, *150*(2), 279–287. Retrieved from https://linkinghub.elsevier.com/retrieve/pii/S0019103500965771 doi: 10.1006/icar.2000.6577

Lee, S., Zanolin, M., Thode, A. M., Pappalardo, R. T., & Makris, N. C. (2003, 9). Probing Europa's interior with natural sound sources. *Icarus*, *165*(1), 144–167. Retrieved from https://linkinghub.elsevier.com/retrieve/pii/S0019103503001507 doi: 10.1016/S0019-1035(03)00150-7

Lognonné, P., Banerdt, W. B., Giardini, D., Pike, W. T., Christensen, U., Laudet, P., ... Wookey, J. (2019, 2). SEIS: Insight's Seismic Experiment for Internal Structure of Mars. *Space Science Reviews*, *215*(1), 12. Retrieved from http://link.springer.com/10.1007/s11214-018-0574-6 doi: 10.1007/s11214-018-0574-6

Lucchetti, A., Pozzobon, R., Mazzarini, F., Cremonese, G., & Massironi, M. (2017, 11). Brittle ice shell thickness of Enceladus from fracture distribution analysis. *Icarus*, *297*, 252–264. Retrieved from http://www.sciencedirect.com/science/article/pii/S001910351630416Xhttps://linkinghub.elsevier.com/retrieve/pii/S001910351630416X doi: 10.1016/j.icarus.2017.07.009

Mackenzie, S. M., Neveu, M., Davila, A. F., Lunine, J. I., Craft, K. L., Cable, M. L., ... Spilker, L. J. (2021). The Enceladus Orbilander Mission Concept : Balancing Return and Resources in the Search for Life. *The Planetary Science Journal*, *2*(2), 77. Retrieved from http://dx.doi.org/10.3847/PSJ/abe4da doi: 10.3847/PSJ/abe4da

Maguire, R. R., Schmerr, N. C., Lekić, V., Hurford, T. A., Dai, L., & Rhoden, A. R. (2021). Constraining Europa's ice shell thickness with fundamental mode surface wave dispersion. *Icarus*, *369*, 114617. Retrieved from https://www.sciencedirect.com/science/article/pii/S0019103521002815 doi: 10.1016/j.icarus.2021.114617

Marusiak, A. G., Panning, M. P., Vance, S. D., Nunn, C., Stähler, S. C., & Tharimena, S. (2022, 6). Seismic Detection of Euroquakes Originating From Europa's Silicate Interior. *Earth and Space Science*, *9*(6). Retrieved from https://onlinelibrary.wiley.com/doi/10.1029/2021EA002041 doi: 10.1029/2021EA002041

Marusiak, A. G., Vance, S. D., Panning, M. P., Běhounková, M., Byrne, P. K., Choblet, G., ... Wang, S. (2021, 8). Exploration of Icy Ocean Worlds Using Geophysical Approaches. *The Planetary Science Journal*, *2*(4), 150. Retrieved from https://iopscience.iop.org/article/10.3847/PSJ/ac1272 doi: 10.3847/PSJ/ac1272

Marusiak, A. G., Vance, S. D., Panning, M. P., Bryant, Andrea, Hesse, M. A., Carnahan, E., & Journaux, B. (2022). The effects of methane clathrates on the thermal and seismic profile of Titan's icy lithosphere. *Planetary Science Journal*, *in revisio*.

Masters, G., Woodhouses, J. H., & Freeman, G. (2011). *Mineos.* Computational Infrastructure of Geodynamics.

McKinnon, W. B. (2015, 4). Effect of Enceladus's rapid synchronous spin on interpretation of Cassini gravity. *Geophysical Research Letters*, *42*(7), 2137–2143. Retrieved from http://doi.wiley.com/10.1002/2015GL063384 doi: 10.1002/2015GL063384

National Academies of Sciences Engineering and Medicine. (2022). *Origins, Worlds, and Life: A decadal Strategy for Planetary Science and Astrobiology 2023-2032*. Washington, D.C.: National Academies Press. Retrieved from https://www.nap.edu/catalog/26522 doi: 10.17226/26522

Olgin, J. G., Smith-Konter, B. R., & Pappalardo, R. T. (2011, 1). Limits of Enceladus's ice shell thickness from tidally driven tiger stripe shear failure. *Geophysical Research Letters*, *38*(2). Retrieved from 10.1029/2010GL044950 doi: https://doi.org/10.1029/2010GL044950

Panning, M. P., Stähler, S. C., Vance, S. D., Kedar, S., Tsai, V. C., Pike, W. T., ... Lorenz, R. D. (2018, 1). Expected seismicity and the seismic noise environment of Europa. *Journal of Geophysical Research: Planets*, *123*(1), 163–179. Retrieved from http://onlinelibrary.wiley.com/doi/10.1002/2017JE005332/abstract doi: 10.1002/2017JE005332

Pappalardo, R. T., Vance, S. D., Bagenal, F., Bills, B. G., Blaney, D. L., Blankenship, D. D., ... Soderlund, K. M. (2013). Science potential from a Europa lander. *Astrobiology*, *13*(8), 740–773. Retrieved from http://www.ncbi.nlm.nih.gov/pubmed/23924246 doi: 10.1089/ast.2013.1003

Stähler, S. C., Panning, M. P., Vance, S. D., Lorenz, R. D., van Driel, M., Nissen-Meyer, T., ... Kedar, S. (2017). Seismic Wave Propagation in Icy Ocean Worlds. *Journal of Geophysical Research: Planets*, *123*(1), 206–232. Retrieved from http://onlinelibrary.wiley.com/doi/10.1002/2017JE005338/abstract doi: 10.1002/2017JE005338

Tajeddine, R., Soderlund, K. M., Thomas, P. C., Helfenstein, P., Hedman, M. M., Burns, J. A., & Schenk, P. M. (2017, 10). True polar wander of Enceladus from topographic data. *Icarus*, *295*, 46–60. Retrieved from

https://linkinghub.elsevier.com/retrieve/pii/S001910351630584X doi: 10.1016/j.icarus.2017.04.019

Vance, S. (2017). *vancesteven/planetprofile: Release for use in reproducing results submitted to Journal of Geophysical Research: Planets, Zenodo.*

Vance, S. D., Behounkova, M., Bills, B. G., Byrne, P., Cadek, O., Castillo-Rogez, J., ... Wang, S. (2021, 3). Distributed Geophysical Exploration of Enceladus and Other Ocean Worlds. *Bulletin of the AAS*, *53*(4), 127. Retrieved from https://baas.aas.org/pub/2021n4i127 doi: 10.3847/25c2cfeb.a07234f4

Vance, S. D., DellaGiustina, D. N., Hughson, K., Hurford, T., Kedar, S., Marusiak, A. G., ... Weber, R. C. (2021, 5). Planetary Seismology: The Solar System's Ocean Worlds. In *Bulletin of the american astronomical society* (Vol. 53, p. 129). Retrieved from https://ui.adsabs.harvard.edu/abs/2021BAAS...53d.129V doi: 10.3847/25c2cfeb.ca102d2f

Vance, S. D., Marusiak, A. G., Daswani, M. M., Styczinski, M. J., Lisitsyn, A., Vega, K., & Bryant, A. (2022). *PlanetProfile: Supplementary Data: Effects of Methane Clathrate Lids on Titan's Ice Shell and added TauP functionality.* doi: 10.5281/zenodo.6323610

Vance, S. D., Panning, M. P., Stähler, S., Cammarano, F., Bills, B. G., Tobie, G., ... Banerdt, B. (2018, 11). Geophysical Investigations of Habitability in Ice-Covered Ocean Worlds. *Journal of Geophysical Research: Planets*, *123*(1), 180–205. Retrieved from http://doi.wiley.com/10.1002/2017JE005341https://doi.org/10.1002/2017JE005341 doi: 10.1002/2017JE005341

Waite, J. H., Glein, C. R., Perryman, R. S., Teolis, B. D., Magee, B. A., Miller, G., ... Bolton, S. J. (2017). Cassini finds molecular hydrogen in the Enceladus plume: Evidence for hydrothermal processes. *Science*, *356*(6334), 155–159. doi: 10.1126/science.aai8703